CHAPTER – IV

VIBRATIONAL SPECTRA OF 4-AMINOPHTHALONITRILE(4APN) AND COMPARATIVE ANALYSIS WITH QUANTUM CHEMICAL CALCULATIONS FOR DYE SENSITIZED SOLAR CELLS

CHAPTER – IV

Vibrational Spectra of 4-Aminophthalonitrile(4APN) and Comparative Analysis with Quantum Chemical Calculations for Dye Sensitized Solar Cells

4.1 Introduction to 4APN

Photoinduced electron transfer at molecular interfaces constitutes a major focus of research in developing solar energy conversion devices since it creates free charge carriers on the absorption of a photon. Dye Sensitized Solar Cell (DSSC) is based on transition due to dye molecules adsorbed to a highly porous nanocrystalline TiO_2. In this chapter a phthalonitrile dye sensitizer 4-Aminophthalonitrile (4APN) (CAS Number: 56765-79-8) is selected for our study. Its molecular formula is $C_8H_5N_3$ and molecular weight is 143.15 [g/mol]. The synonym of this dye is 3,4-Dicyanoaniline. The performance of this metal free dye that can be used in DSSC is studied using the vibrational spectral analysis.

4.2 Experimental Details for 4APN

The compound 4APN was taken with a stated purity of greater than 99% and it was used as such without further purification. The FT-Raman spectrum of 4APN has been recorded using 1064 nm line of Nd:YAG laser as excitation wavelength in the region 50-3500 cm^{-1} on a Brucker model IFS 66 V spectrophotometer. The FT-IR spectrum of this compound was recorded in the region 400-4000 cm^{-1} on IFS 66 V spectrophotometer using KBr pellet technique. The spectrum was recorded at room temperature, with scanning speed of 30 $cm^{-1}min^{-1}$ and the spectral resolution of 2.0 cm^{-1}.

4.3 Computational methods for 4APN

The computations of the geometries, electronic structures, polarizabilities and hyperpolarizabilities, as well as electronic absorption spectrum for dye sensitizer 4APN was done using Hartree-Fock (HF) and Density Functional Theory (DFT) with Gaussian 03 package [1]. The DFT was treated with hybrid functional Becke's three parameter and the Lee-Yang-Parr potential (B3LYP) [2-4], and all calculations were performed without any symmetry constraints by using polarized split-valence 6-311++G(d,p) basis sets. The NBO analysis were performed using Restricted Hartree Fock (RHF) with the 6-311++G(d,p) basis sets. The electronic absorption spectrum requires calculation of the allowed excitations and oscillator strengths. These calculations were done using TD-DFT with the Perdew-Burke-Ernzerhof exchange-correlation functional (PBE1PBE) applied to 6-311++G(d,p) basis set in vacuum and acetonitrile solution, and the non-equilibrium version of the Polarizable Continuum Model (PCM) [5,6] was adopted for calculating the solvent effects.

4.4 Results and discussion

4.4.1 The geometric structure of 4APN

The optimized geometry of the 4APN is shown in Figure 4.1, and the bond lengths, bond angles and dihedral angles are listed in Table 4.1. From the theoretical values we can find the optimized bond lengths, bond angles and dihedral angles. The distance between C2 and C3 atoms in cyanine groups of 4APN are 1.4412 and 1.4423 Å respectively at B3LYP / 6-311++G (d,p) and also compared with HF / 6-311++G (d,p).

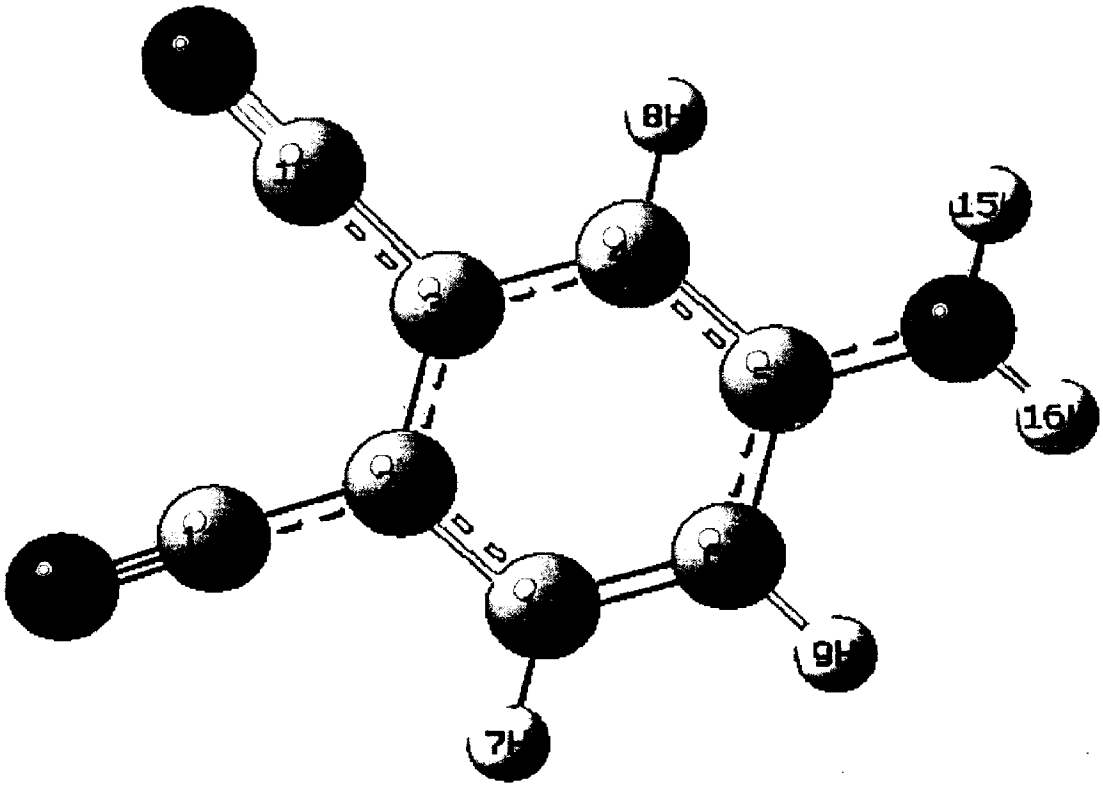

Figure 4.1 Optimized geometrical structure of dye 4APN

Table 4.1 Bond lengths (in Å), bond angles (in degree) and dihedral angles (in degree) of the dye 4APN

Parameters	HF/6-311++G(d,p)	B3LYP/6-311++G(d,p)
Bond length(Å)		
C1-C2	1.3860	1.4024
C1-C6	1.3820	1.3831
C1-H7	1.0736	1.0828
C2-C3	1.3949	1.4131
C2-C11	1.4412	1.4255
C3-C4	1.3855	1.3937
C3-C10	1.4423	1.4314
C4-C5	1.3860	1.4039
C4-H8	1.0727	1.0834
C5-C6	1.3882	1.4073
C5-N14	1.4255	1.3774
C6-H9	1.0754	1.0844
C10-N12	1.1294	1.1548
C11-N13	1.1296	1.1560
N14-H15	1.0000	1.0075
N14-H16	1.0000	1.0073
Bond angles (°)		
C2-C1-C6	120.2	121.2
C2-C1-H7	119.3	118.9
C6-C1-H7	120.4	119.8
C1-C2-C3	119.3	118.2
C1-C2-C11	119.1	119.9
C3-C2-C11	121.5	121.8
C2-C3-C4	120.0	120.4
C2-C3-C10	121.1	120.9
C4-C3-C10	118.8	118.5
C3-C4-C5	120.6	120.8

Table 4.1 (Contd..) Bond lengths (in Å), bond angles (in degree) and dihedral angles (in degree) of the dye 4APN

Parameters	HF/6-311++G(d,p)	B3LYP/6-311++G(d,p)
Bond angles (°)		
C3-C4-H8	120.2	119.0
C5-C4-H8	119.0	120.1
C4-C5-C6	118.9	118.4
C4-C5-N14	118.0	120.5
C6-C5-N14	123.0	120.9
C1-C6-C5	120.8	120.7
C1-C6-H9	119.5	119.6
C5-C6-H9	119.6	119.6
C5-N14-H15	111.4	118.4
C5-N14-H16	111.4	118.3
H4-N14-H16	108.1	114.7
Dihedral angles (°)		
C6-C1-C2-C3	0.0038	0.0150
C6-C1-C2-C11	-179.9987	-179.895
H7-C1-C2-C3	180.0011	179.953
H7-C1-C2-C11	-0.0014	0.0431
C2-C1-C6-C5	-0.0032	0.0423
C2-C1-C6-H9	179.9971	-179.7667
H7-C1-C6-C5	179.9996	-179.8952
H7-C1-C6-H9	-0.0002	0.2958
C1-C2-C3-C4	-0.0008	0.0003
C1-C2-C3-C10	179.9976	-179.9188
C11-C2-C3-C4	-179.9982	179.9084
C11-C2-C3-C10	0.0002	-0.0107
C2-C3-C4-C5	-0.0029	-0.0731
C2-C3-C4-H8	179.9957	179.7877
C10-C3-C4-C5	179.9986	179.8479

Table 4.1 (Contd..) Bond lengths (in Å), bond angles (in degree) and dihedral angles (in degree) of the dye 4APN

Parameters	HF/6-311++G(d,p)	B3LYP/6-311++G(d,p)
Dihedral angles (°)		
C10-C3-C4-H8	-0.0028	-0.2913
C3-C4-C5-C6	0.0035	0.1279
C3-C4-C5-N14	-180.0003	177.8726
H8-C4-C5-C6	-179.9951	-179.7314
H8-C4-C5-N14	0.0011	-1.9867
C4-C5-C6-C1	-0.0005	-0.1126
C4-C5-C6-H9	-180.0007	179.6963
N14-C5-C6-C1	-179.9965	-177.8493
N14-C5-C6-H9	0.0032	1.9596
C4-C5-N14-H15	119.4136	17.8279
C4-C5-N14-H16	-119.6282	164.2982
C6-C5-N14-H15	-60.5904	-164.484
C6-C5-N14-H16	60.3678	-18.0137

4.4.2. Electronic structures and charges of 4APN

Natural Bond Orbital (NBO) analysis was performed in order to analyze the charge populations of the dye 4APN. Charge distributions in C, N and H atoms were observed because of the different electro-negativity, the electrons transferred from C atoms to C, N atoms, C atoms to H and N atoms to H atom. The natural charges of different groups are the sum of every atomic natural charge in the group. These data indicate that the cyanine groups are donors and amide groups is acceptor and the atomic charges were transferred through chemical bonds. The frontier molecular orbitals (MO) energies and corresponding density of state of the dye 4APN is shown in Figure 4.2. The HOMO–LUMO gap of the dye 4APN in vacuum is 5.57 eV. While the calculated HOMO

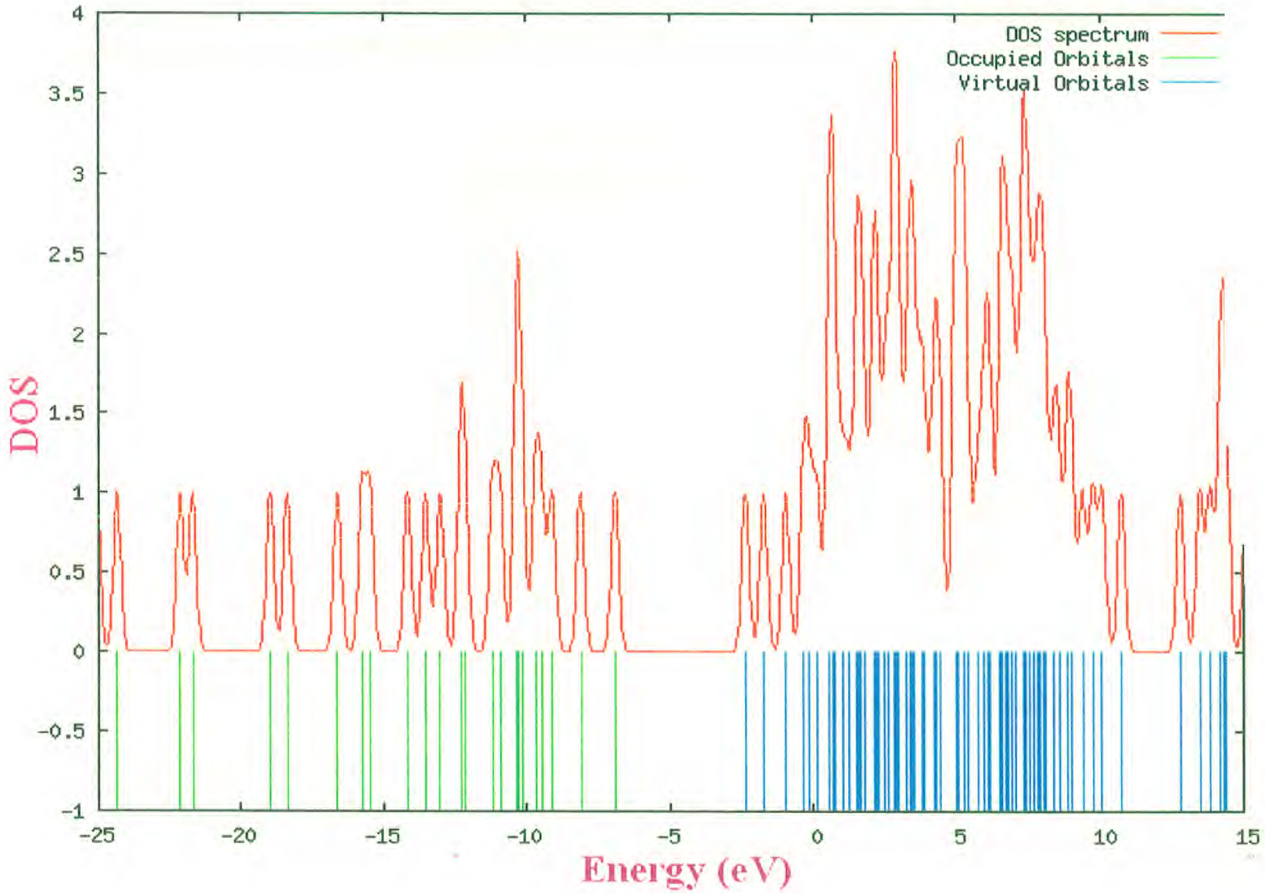

Figure 4.2 The frontier molecular orbital energies and corresponding density of state (DOS) spectrum of the dye 4APN

and LUMO energies of the bare $Ti_{38}O_{76}$ cluster as a model for nanocrystalline are -6.55 and -2.77eV, respectively, resulting in a HOMO–LUMO gap of 3.78 eV, the lowest transition is reduced to 3.20 eV according to TD-DFT, and this value is slightly smaller than typical band gap of TiO_2 nanoparticles with nm size [7]. Furthermore, the HOMO, LUMO and HOMO–LUMO gap of $(TiO_2)_{60}$ cluster is -7.52, -2.97, and 4.55 eV (B3LYP/VDZ), respectively [8]. Taking into account of the cluster size effects and the calculated HOMO, LUMO, HOMO–LUMO gap of the dye 4APN, $Ti_{38}O_{76}$ and $(TiO_2)_{60}$ clusters, we can find that the HOMO energies of these dyes fall within the TiO_2 gap. The above data also reveal the interfacial electron transfer between semiconductor TiO_2 electrode and the dye sensitizer 4APN is electron injection processes from excited dye to the semiconductor conduction band. This is a kind of typical interfacial electron transfer reaction [9].

4.4.3. Polarizability and hyperpolarizability of 4APN

Polarizabilities and hyperpolarizabilities characterize the response of a system in an applied electric field [10]. They determine not only the strength of molecular interactions (long-range intermolecular induction, dispersion forces, etc.) as well as the cross sections of different scattering and collision processes, but also the nonlinear optical properties (NLO) of the system [11,12]. It has been found that the dye sensitizer hemicyanine system, which has high NLO property, usually possesses high photoelectric conversion performance [13]. In order to investigate the relationships among photocurrent generation, molecular structures and NLO, the polarizabilities and hyperpolarizabilities of 4APN was calculated. Here, the polarizability and the first hyperpolarizabilities are computed using B3LYP / 6-311++G(d,p). The definitions [11,12] for the isotropic polarizability is

$$\alpha = \frac{1}{3}(\alpha_{XX} + \alpha_{YY} + \alpha_{ZZ}) \tag{4.1}$$

The polarizability anisotropy invariant is

$$\Delta\alpha = \left[\frac{(\alpha_{XX} - \alpha_{YY})^2 + (\alpha_{YY} - \alpha_{ZZ})^2 + (\alpha_{ZZ} - \alpha_{XX})^2}{2}\right]^{\frac{1}{2}} \tag{4.2}$$

and the average hyperpolarizability is

$$\beta_{ii} = \frac{1}{5}\sum_i(\beta_{iiZ} + \beta_{iZi} + \beta_{Zii}) \tag{4.3}$$

where, α_{XX}, α_{YY}, and α_{ZZ} are tensor components of polarizability; β_{iiZ}, β_{iZi}, and β_{Zii} (i from X to Z) are tensor components of hyperpolarizability. Tables 4.2 and 4.3 list the values of the polarizabilities and hyperpolarizabilities of the dye 4APN.

Table 4.2 Polarizability (α) of the dye 4APN (in a.u.)

α_{xx}	α_{xy}	α_{yy}	α_{xz}	α_{yz}	α_{zz}	α	Δα
169.1	1.5	120.2	-0.3	-0.1	57.2	115.5	97.2

Table 4.3 Hyperpolarizability (β) of the dye 4APN (in a.u.)

β_{xxx}	β_{xxy}	β_{xyy}	β_{yyy}	β_{xxz}	β_{xyz}	β_{yyz}	β_{xzz}	β_{yzz}	β_{zzz}	β_{ii}
-663.5	-265.7	-14.7	96.7	12.5	2.9	3.6	64.9	-15.8	7.5	14.2

In addition to the individual tensor components of the polarizabilties and the first hyperpolarizabilities, the isotropic polarizability, polarizability anisotropy invariant and hyperpolarizability are also calculated. The calculated isotropic polarizability of 4APN is 115.5 a.u. However, the calculated isotropic polarizability of JK16, JK17, dye 1, dye 2, D5, DST and DSS is 759.9, 1015.5, 694.7, 785.7, 510.6, 611.2 and 802.9 a.u., respectively [14,15]. The above data indicate that the donor-conjugate π bridge-acceptor (D-π-A) chain-like dyes have stronger response for external electric field. Whereas, for dye sensitizers D5, DST, DSS, JK16, JK17, dye 1 and dye 2, on the basis of the published photo-to-current conversion efficiencies, the similarity and the difference of geometries, and the calculated isotropic polarizabilities, it is found that the longer the length of the conjugate bridge in similar dyes, the larger the polarizability of the dye molecule, and the lower the photo-to-current conversion efficiency. This may be due to the fact that the longer conjugate π bridge enlarged the delocalization of electrons, thus it enhanced the response of the external field, but the enlarged delocalization may be not favorable to generate charge separated state effectively. So it induces the lower photo-to-current conversion efficiency.

4.4.4 IR and Raman frequencies of 4APN

Figure 4.3 and 4.4 shows the observed and calculated IR and Raman spectra of 4APN respectively. Comparison of the observed (FT-IR and FT-Raman) and calculated vibrational frequencies of 4APN is shown in Table 4.4. Comparison of the frequencies calculated by ab initio HF and B3LYP with experimental values reveals the overestimation of the calculated vibrational modes due to neglect of anharmonicity in real system. Inclusion of electron correlation in density functional theory to a certain extent makes the frequency values smaller in comparison with experimental values. Any way notwithstanding the level of calculations it is customary to scale down the calculated

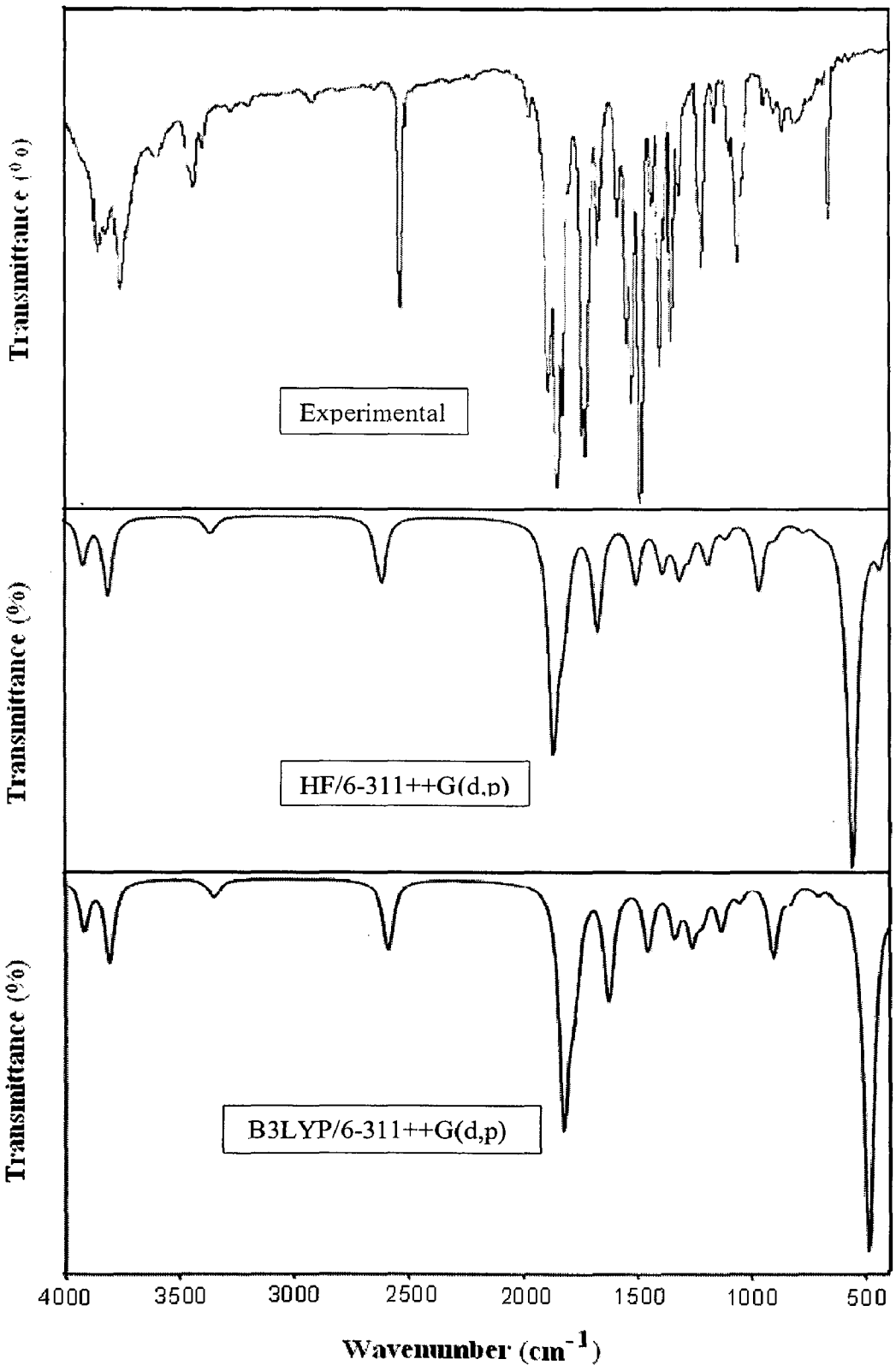

Figure 4.3 Observed and Calculated FT-IR Spectra of 4APN

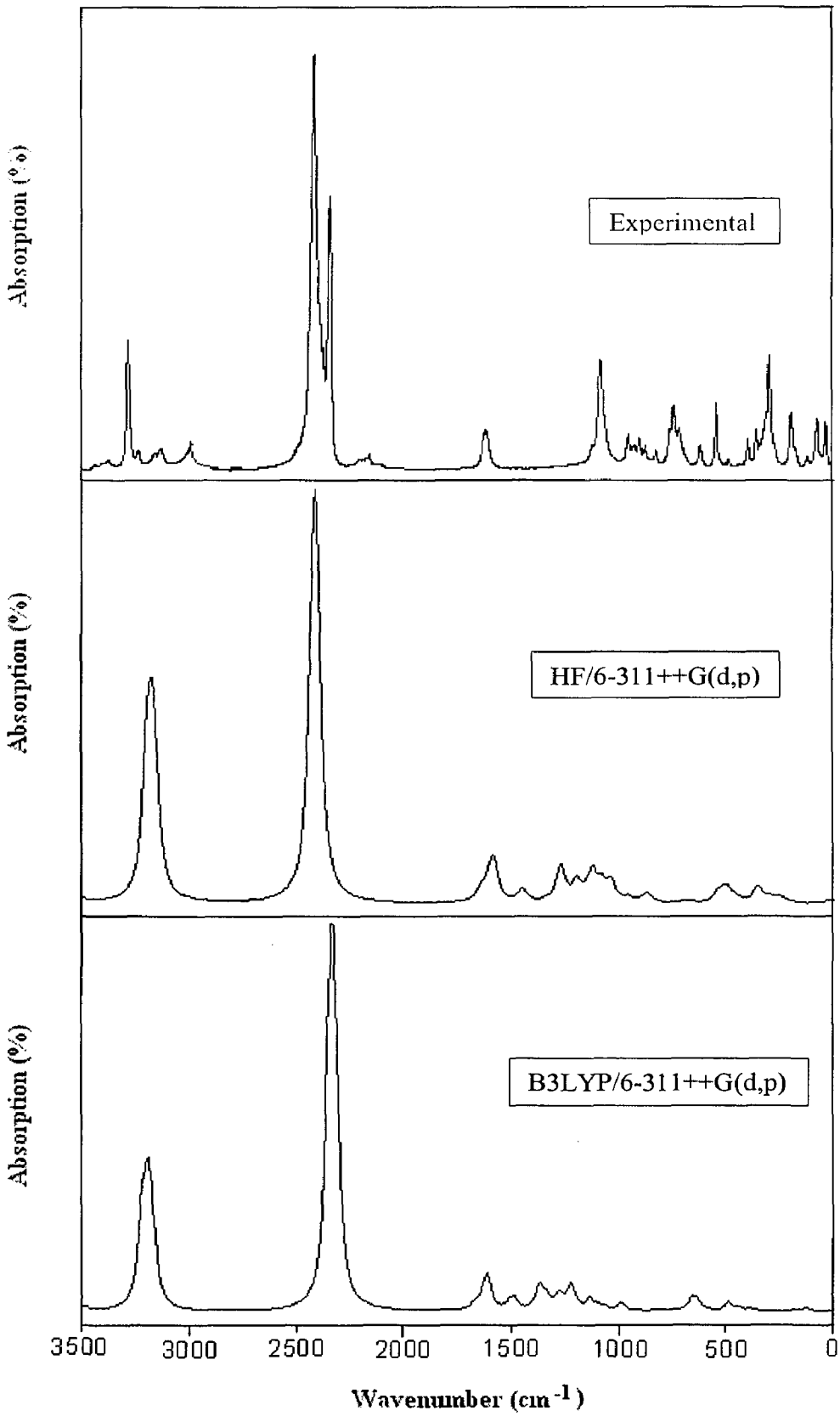

Figure 4.4 Observed and Calculated FT-Raman Spectra of 4APN

Table 4.4 Comparison of the observed (FT-IR and FT-Raman) and calculated vibrational frequencies of 4APN

Vibrational mode no.	Species	Experimental Wavenumber (cm^{-1})		Scaled Wavenumber (cm^{-1})		IR Intensity (KM/Mole)	Raman active (A^4/AMU)	Assignments	PED (%)
		FT-IR	FT-Raman	HF/6-311++G (d,p)	B3LYP/6-311++G (d,p)				
1	A'	-	-	105	94	0.2	0.4	β C-C-N	β C-C-N (94)
2	A'	-	124	131	118	1.5	6.8	β C-C-N	β C-C-N (79)
3	A''	-	-	158	142	1.3	0.1	γ C-C-N	γ C-C-N (85)
4	A''	-	-	192	175	3.2	0.3	γ C-C-N	γ C-C-N (96)
5	A''	-	-	280	253	7.9	0.0	γ C-C-N	γ C-C-N (65)
6	A''	-	-	331	359	13.1	0.0	τ C-C-C + γ C-C-N	τ C-C-C (24) + γ C-C-N(45)
7	A'	-	-	404	375	2.7	2.3	τ C-C-C	τ C-C-C (68)
8	A''	422	-	430	387	314.8	5.2	γ C=C	γ C=C (93)
9	A''	445	-	432	391	19.4	1.5	τ C-C-C	τ C-C-C (74)
10	A'	-	-	495	405	1.8	5.6	Ring deformation	-
11	A'	-	-	499	459	2.4	1.2	Ring deformation	-
12	A'	-	480	543	466	2.1	13.8	Ring deformation	-
13	A'	-	-	596	544	1.3	2.2	β C-C-N	β C-C-N (76)
14	A'	591	-	608	548	13.6	3.4	β C-C-N	β C-C-N (71)
15	A'	-	-	694	641	0.7	1.6	β C-C-N	β C-C-N (93)

Table 4.4 (Contd.) Comparison of the observed (FT-IR and FT-Raman) and calculated vibrational frequencies of 4APN

Vibrational mode no.	Species	Experimental Wavenumber (cm^{-1})		Scaled Wavenumber (cm^{-1})		IR Intensity (KM/Mole)	Raman active (A^4/AMU)	Assignments	PED (%)
		FT-IR	FT-Raman	HF/6-311++G (d,p)	B3LYP/6-311++G (d,p)				
16	A'	-	-	712	643	2.7	1.1	β C-C-N	β C-C-N (78)
17	A'	-	743	776	730	1.1	10.2	Ring deformation	-
18	A'	-	749	781	735	3.5	13.2	Ring deformation	-
19	A''	-	-	809	739	0.3	0.7	γ C-H	γ C-H (64)
20	A'	874	-	934	838	30.2	0.1	Ring deformation	-
21	A''	906	-	977	881	17.5	0.4	ω C-H	ω C-H (54)
22	A''	-	985	1018	957	2.1	25.8	ω C-H	ω C-H (91)
23	A'	-	-	1089	973	1.1	0.2	Ring deformation	-
24	A'	-	-	1161	1079	2.0	3.1	β C-H	β C-H (89)
25	A''	1169	-	1194	1126	17.0	5.1	γ C-H	γ C-H (68)
26	A'	-	1219	1260	1197	2.41	12.2	β C-H	β C-H (95)
27	A'	-	1240	1313	1236	0.6	57.7	β C-H	β C-H (99)
28	A'	1298	1311	1328	1283	38.1	22.7	υ C=C	υ C=C (90)
29	A'	-	-	1385	1341	6.6	6.2	Ring deformation	-
30	A'	1407	1383	1441	1352	92.6	27.5	υ_{sym} C=C	υ_{sym} C=C (98)

Table 4.4 (Contd.) Comparison of the observed (FT-IR and FT-Raman) and calculated vibrational frequencies of 4APN

Vibrational mode no.	Species	Experimental Wavenumber (cm^{-1})		Scaled Wavenumber (cm^{-1})		IR Intensity (KM/Mole)	Raman active (A^4/AMU)	Assignments	PED (%)
		FT-IR	FT-Raman	HF/6-311++G (d,p)	B3LYP/6-311++G (d,p)				
31	A'	-	-	1590	1469	5.1	7.7	υ C=C	υ C=C (97)
32	A'	1518	1562	1665	1530	56.3	44.5	υ_{asy} C=C	υ_{asy} C=C (97)
33	A'	1580	1584	1748	1591	17.7	22.5	υ_{asy} C=C	υ_{asy} C=C (91)
34	A'	1636	1633	1780	1641	116.2	116.2	υ_{sym} C=C	υ_{sym} C=C (93)
35	A'	1661	-	1814	1666	265.3	54.4	υ_{sym} C=C	υ_{sym} C=C (87)
36	A'	2312	2340	2586	2329	55.9	679.9	υ_{asy} C-N	υ_{asy} C-N (98)
37	A'	2319	2368	2598	2340	12.5	361.3	υ C-N	υ C-N (90)
38	A'	-	3196	3334	3173	6.8	94.6	υ_{asy} C-H	υ_{asy} C-H (93)
39	A'	-	3204	3351	3186	2.9	68.4	υ C-H	υ C-H (97)
40	A'	-	3219	3363	3200	1.3	126.5	υ_{asy} C-H	υ_{asy} C-H (96)
41	A'	3574	3642	3802	3595	82.5	272.9	υ_{sym} C-H	υ_{sym} C-H (85)
42	A'	3678	3761	3909	3701	33.3	61.7	υ_{sym} C-H	υ_{sym} C-H (92)

υ - stretching; υ_{sym} - symmetric stretching ; υ_{asy}-asymmetric stretching; β-in plane bending; γ- out-of-plane bending; ω-wagging; τ- torsion

harmonic frequencies in order to improve the agreement with the experiment.

In our study we have followed two different scaling factors B3LYP/ 6-311++G(d,p) and HF/6-311++G(d,p). The 4APN molecule give rise to six C-C-N inplane bending vibrations at 94, 118, 544, 548, 641 and 643 cm^{-1}, four C-C-N out-of plane bending vibration at 142, 175, 253 and 359 cm^{-1}, three C-C-C torsion at 359, 375 and 391 cm^{-1}, one C=C out-of plane bending vibration at 387 cm^{-1}, eight ring deformations at 405, 459, 466, 730, 735, 838, 973 and 1341 cm^{-1}, two CH out-of plane bending vibrations at 739 and 1126 cm^{-1}, two CH wagging at 881 and 957 cm^{-1}, three CH inplane bending vibrations at 1079, 1197 and 1236 cm^{-1}, two C=C stretching vibrations at 1283 and 1469 cm^{-1}, three C=C symmetrical stretching vibrations at 1352, 1641 and 1666 cm^{-1}, two C=C asymmetrical stretching vibrations at 1530 and 1591 cm^{-1}, one C≡N asymmetrical stretching vibration at 2329 cm^{-1}, one C≡N stretching vibration at 2340 cm^{-1}, two C-H asymmetrical stretching vibrations at 3173 and 3200 cm^{-1}, one C-H stretching vibration at 3186 cm^{-1} and two C-H asymmetrical stretching vibrations at 3595 and 3701 cm^{-1} were assigned. The strongest IR absorption for 4APN corresponds to the vibrational mode 8 near about 387 cm^{-1}, which is the wagging mode of C-H bonds. The next stronger IR absorption is attributed to vibrational mode 35 near about 1666 cm^{-1}, corresponding to stretching mode of C=C bonds. In the Raman spectra, however, the strongest activity mode is the vibrational mode 36 near about 2329 cm^{-1}, which is corresponding to stretching mode of C-N triple bond.

4.4.5 Electronic absorption spectra and sensitized mechanism of 4APN

Electronic absorption spectra of 4APN in vacuum and solvent were performed using TD-DFT(PBE1PBE)/6-311++G(d,p) calculations, and the results are shown in Figure 4.5. It is observed that the absorption in the visible region is much weaker than that in the UV region for 4APN. The results of TD-DFT have an appreciable red-shift in

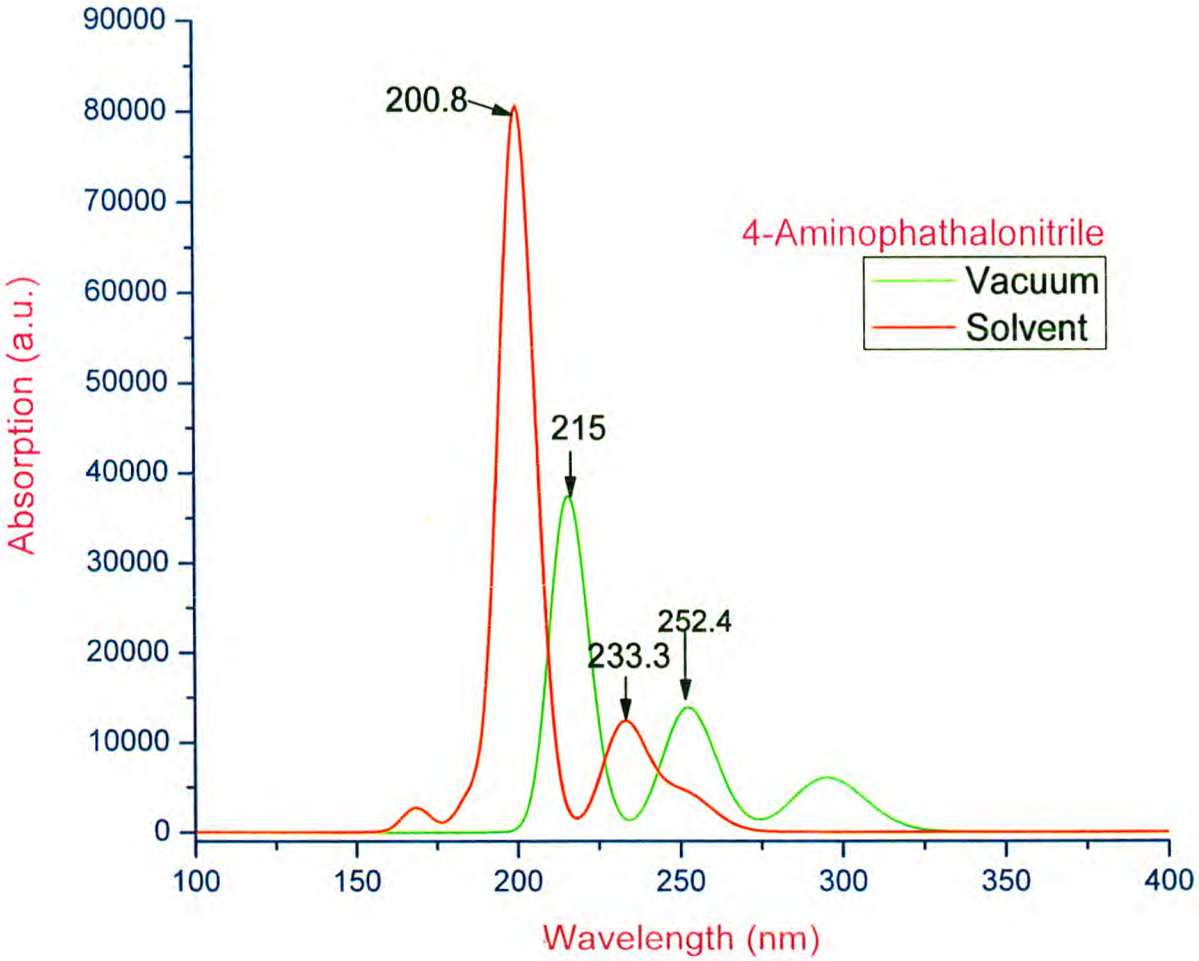

Figure 4.5 Calculated electronic absorption spectra of the dye 4APN

vacuum and solvent, and the degree of red-shift in solvent is more significant than that in vacuum.

The discrepancy between vacuum and solvent effects in TD-DFT calculations may result from two aspects. The first aspect is smaller gap of materials which induces smaller excited energies. The other is solvent effects. Experimental measurements of electronic absorptions are usually performed in solution. Solvent, especially polar solvent, could affect the geometry and electronic structure as well as the properties of molecules through the long-range interaction between solute molecule and solvent molecule. For these reasons it is more difficult to make the TD-DFT calculation is consistent with quantitatively. Though the discrepancy exists, the TD-DFT calculations are capable of describing the spectral features of 4APN because of the agreement of lineshape and relative strength as compared with the vacuum and solvent. The HOMO-LUMO gap of 4APN in acetonitrile at PBE1PBE / 6-311++G (d,p) theory level is smaller than that in vacuum.This fact indicates that the solvent effects stabilize the frontier orbitals of 4APN. So it induces the smaller intensities and red-shift of the absorption as compared with that in vacuum.

In order to obtain the microscopic information about the electronic transitions, the corresponding MO properties are checked. The absorption in visible and near-UV region is the most important region for photo-to-current conversion, so only the 20 lowest singlet/singlet transitions of the absorption band in visible and near-UV region for 4APN is listed in Table 4.5. The data of Table 4.5 and Figure 4.6 are based on the 6-311++G (d,p) results with solvent effects involved.

This indicates that the transitions are photoinduced charge transfer processes, thus the excitations generate charge separated states, which should favour the electron injection from the excited dye to semiconductor surface.

Table 4.5 Computed excitation energies, electronic transition configurations and oscillator strengths (f) for the optical transitions of the absorption bands in visible and near- UV region for the dye 4APN in acetonitrile

State	Configurations composition (corresponding transition orbital)	Excitation energy (eV/nm)	Oscillator strength (f)
1	0.70217(37 → 38)	4.2211 / 293.72	0.0000
2	0.70250(37 → 39)	4.8285 / 256.77	0.0000
3	0.43727 (35 → 38) 0.22590 (35 → 39) -0.39397 (36 → 38) 0.31754 (36 → 39)	4.9353 / 251.22	0.0560
4	0.38409 (35 → 38) -0.13962 (35 → 39) 0.48208 (36 → 38) 0.20025 (36 → 39)	5.3301 / 232.61	0.1684
5	-0.30329 (35 → 38) 0.12425 (35 → 39) 0.51214 (36 → 39)	6.1720 / 200.88	0.8716
6	-0.11828 (33 → 38) 0.57670 (35 → 39) 0.17277 (36 → 38) -0.16100 (36 → 39)	6.3141 / 196.36	0.3295
7	0.59091(34 → 38) -0.10525(35 → 40) -0.31215(36 → 40)	6.6383 / 186.77	0.0000
8	0.69804 (37 → 40)	6.7036 / 184.95	0.0527
9	0.33051(34 → 38) 0.10288(35 → 40) 0.58467(36 → 40)	6.7224 / 184.43	0.0001
10	0.65360(32 → 38) -0.14751(34 → 39) -0.13950(35 → 40)	6.7658 / 183.25	0.0000
11	0.15208(32 → 38) 0.64205(35 → 40) -0.11500(35 → 41) -0.14580(36 → 40) 0.11930(36 → 41)	6.8902 / 179.94	0.0000
12	0.65463(33 → 38) 0.15116(34 → 40)	7.0992 / 174.65	0.0036
13	0.59653 (37 → 41) -0.28828 (37 → 42) -0.22864 (37 → 45)	7.3004 / 169.83	0.0205

Table 4.5 (Contd..) Computed excitation energies, electronic transition configurations and oscillator strengths (f) for the optical transitions of the absorption bands in visible and near- UV region for the dye 4APN in acetonitrile

State	Configurations composition (corresponding transition orbital)	Excitation energy (eV/nm)	Oscillator strength (f)
14	-0.16321(28 → 38) -0.25672(29 → 38) 0.52142(30 → 38) -0.26502(34 → 39) 0.16430(36 → 41)	7.3538 / 168.60	0.0001
15	-0.17142(30 → 38) 0.11898(35 → 40) -0.12813(36 → 40) 0.63716(36 → 41)	7.4245 / 166.99	0.0000
16	0.35409 (37 → 41) 0.57388 (37 → 42) 0.17051 (37 → 45)	7.4304 / 166.86	0.0106
17	0.66053(31 → 38) 0.14783(32 → 40) -0.12436(34 → 41)	7.4661 / 166.06	0.0050
18	0.12120(27 → 38) 0.45398(29 → 38) 0.38115(30 → 38) 0.28350(34 → 39) -0.13331(36 → 42)	7.5218 / 164.83	0.0050
19	-0.13551(29 → 38) -0.10924(32 → 39) 0.19948(34 → 39) 0.17503(35 → 41) 0.21445(37 → 43) 0.55925(37 → 44)	7.5746 / 163.68	0.0001
20	-0.19753(32 → 39) 0.12447(34 → 39) 0.11149(35 → 40) 0.55378(35 → 41) -0.11336(37 → 43) -0.26198(37 → 44)	7.5936 / 163.28	0.0011

The solar energy to electricity conversion efficiency (η) under AM 1.5 white-light irradiation can be obtained from the following formula:

$$\eta(\%) = \frac{J_{SC}[mAcm^{-2}]V_{OC}[V]ff}{I_0[mWcm^{-2}]} \times 100 \qquad (4.4)$$

where I_0 is the photon flux, *Jsc* is the short-circuit photocurrent density, and *Voc* is the

HOMO-3

-9.79

LUMO+3

-0.35

HOMO-2

-8.38

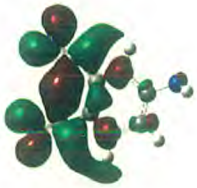

LUMO+2

-0.87

HOMO-1

-8.20

LUMO+1

-2.00

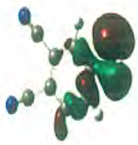

HOMO

-8.08

LUMO

-2.50

Figure 4.6 Isodensity plots (isodensity contour = 0.02 a.u.) of the frontier orbitals and orbital energies (in eV) of the dye 4APN

open-circuit photovoltage, and *ff* represents the fill factor [16]. At present, the *Jsc*, the *Voc*, and the *ff* are only obtained by experiment, the relationship among these quantities and the electronic structure of dye is still unknown. The analytical relationship between Voc and E_{LUMO} may exist. According to the sensitized mechanism (electron injected from the excited dyes to the semiconductor conduction band) and single electron and single state approximation, there is an energy relationship:

$$eV_{oc} = E_{LUMO}-E_{CB} \tag{4.5}$$

where, E_{CB} is the energy of the semiconductor's conduction band edge.

The Voc may be obtained applying the following formula:

$$V_{oc} = \frac{(E_{LUMO}-E_{CB})}{e} \tag{4.6}$$

It induces that the higher the E_{LUMO}, the larger the V_{oc}. The results of organic dye sensitizer JK16 and JK17 [39], D-ST and D-SS also proved the tendency [17] (JK16: E_{LUMO} = -2.73 eV, V_{oc} = 0.74 V; JK17: E_{LUMO} = -2.87 eV, V_{oc} = 0.67 V; D-SS: E_{LUMO} = -2.91 eV, V_{oc} = 0.70 V; D-ST: E_{LUMO} = -2.83 eV, V_{oc} = 0.73 V). Certainly, this formula expects further test by experiment and theoretical calculation. The J_{sc} is determined by two processes, one is the rate of electron injection from the excited dyes to the conduction band of semiconductor, and the other is the rate of redox between the excited dyes and electrolyte. Electrolyte effect on the redox processes is very complex, and it is not taken into account in the present calculations. This indicates that most of excited states of 4APN have larger absorption coefficient, and then with shorter lifetime for the excited states, so it results in the higher electron injection rate which leads to the larger Jsc of 4APN. On the basis of above analysis, it is clear that the 4APN has better performance in DSSC.

4.5. Conclusion

The geometries, electronic structures, polarizabilities, and hyperpolarizabilities of dye 4-Aminophthalonitrile was studied by using ab initio HF and density functional theory with hybrid functional B3LYP, and the UV-Vis spectra were investigated by using TD-DFT methods. The NBO results suggest that 4APN is a (D-π-A) system. The calculated isotropic polarizability of 4APN is 115.5 a.u. The calculated polarizability anisotropy invariant of 4APN is 97.2 a.u. The hyperpolarizability of 4APN is 14.2 a.u. The strongest IR absorption for 4APN corresponds to the vibrational mode 8 near about 387 cm^{-1}, which is the wagging mode of C-H bonds. The next stronger IR absorption is attributed to vibrational mode 35 near about 1666 cm^{-1}, corresponding to stretching mode of C=C bonds. In the Raman spectra, however, the strongest activity mode is the vibrational mode 36 near about 2329 cm^{-1}, which is corresponding to stretching mode of C-N triple bond. The electronic absorption spectral features in visible and near-UV region were assigned based on the qualitative agreement to TD-DFT calculations. The absorptions are all ascribed to $\pi \rightarrow \pi^*$ transition. The three excited states with the lowest excited energies of 4APN is photoinduced electron transfer processes that contributes sensitization of photo-to-current conversion processes. The interfacial electron transfer between semiconductor TiO_2 electrode and dye sensitizer 4APN is electron injection process from excited dye as donor to the semiconductor conduction band. Based on the analysis of geometries, electronic structures, and spectrum properties between 4APN the role of cyanine and amine group in phthalonitrile is as follows: it enlarged the distance between electron donor group and semiconductor surface, and decreased the timescale of the electron injection rate, resulted in giving lower conversion efficiency. This indicates that the choice of the appropriate conjugate bridge in dye sensitizer is very important to improve the performance of DSSC.

References

[1] M.J. Frisch, G.W. Trucks, H.B. Schlegel, G.E. Scuseria, M.A. Robb, J.R. Cheeseman, J.A. Montgomery Jr., T. Vreven, K.N. Kudin, J.C. Burant, J.M. Millam, S.S. Iyengar, J. Tomasi, V. Barone, B. Mennucci, M. Cossi, G. Scalmani, N. Rega, G.A. Petersson, H. Nakatsuji, M. Hada, M. Ehara, K. Toyota, R. Fukuda, J. Hasegawa, M. Ishida, T. Nakajima, Y. Honda, O. Kitao, H. Nakai, M. Klene, X. Li, J.E. Knox, H.P. Hratchian, J.B. Cross, C. Adamo, J. Jaramillo, R. Gomperts, R.E. Stratmann, O. Yazyev, A.J. Austin, R. Cammi, C. Pomelli, J.W. Ochterski, P.Y. Ayala, K. Morokuma, G.A. Voth, P. Salvador, J.J. Dannenberg, V.G. Zakrzewski, S.Dapprich, A.D. Daniels, M.C. Strain, O. Farkas, D.K. Malick, A.D. Rabuck, K. Raghavachari, J.B. Foresman, J.V. Ortiz, Q. Cui, A.G. Baboul, S. Clifford, J.Cioslowski, B.B. Stefanov, G. Liu, A. Liashenko, P. Piskorz, I. Komaromi, R.L. Martin, D.J. Fox, T. Keith, M.A. Al-Laham, C.Y. Peng, A. Nanayakkara, M. Challacombe, P.M.W. Gill, B. Johnson, W. Chen, M.W. Wong, C. Gonzalez, J.A. Pople, Gaussian 03, Gaussian, Inc., Pittsburgh, PA, 2003.

[2] A.D. Becke, J. Chem. Phys. 98 (1993) 5648-5652.

[3] B. Miehlich, A. Savin, H. Stoll, H. Preuss, Chem. Phys. Lett. 157 (1989) 200-206.

[4] C. Lee, W. Yang, R.G. Parr, Phys. Rev. B. 37 (1988) 785-789.

[5] V. Barone, M. Cossi, J. Phys. Chem. A, 102 (1998) 1995-2001.

[6] M. Cossi, N. Rega, G. Scalmani, V. Barone, J. Comput. Chem. 24 (2003) 669-681.

[7] M.K. Nazeeruddin, F. De Angelis, S. Fantacci, A. Selloni, G. Viscardi, P. Liska, S.Ito, B. Takeru, M. Gratzel, J. Am. Chem. Soc. 127 (2005) 16835-16847.

[8] M.J. Lundqvist, M. Nilsing, P. Persson, S. Lunell, Int. J. Quantum Chem. 106 (2006) 3214-3234.

[9] D.F. Waston, G.J. Meyer, Annu. Rev. Phys. Chem. 56 (2005) 119-156.

[10] C. R. Zhang, H. S. Chen, and G. H. Wang, Chem. Res. Chin. U. 20 (2004) 640-646.

[11] Y. Sun, X. Chen, L. Sun, X. Guo, W. Lu, Chem.Phys. Lett. 381 (2003) 397-403.

[12] O. Christiansen, J. Gauss, J. F. Stanton, Chem.Phys. Lett. 305 (1999) 147-155.

[13] Z. S. Wang, Y. Y. Huang, C. H. Huang, J. Zheng, H.M. Cheng, S. J. Tian, Synth. Met. 14 (2000) 201-207.

[14] C.R. Zhang, Y.Z. Wu, Y.H. Chen, H.S. Chen, Acta Phys. Chim. Sin. 25 (2009) 53-60.

[15] A. Seidl, A. Gorling, P. Vogl, J. A. Majewski, M. Levy, Phys. Rev. B 53 (1996) 3764-3774.

[16] K. Hara, T. Sato, R. Katoh, A. Furube, Y. Ohga, A. Shinpo, S. Suga, K. Sayama, H.Sugihara, H. Arakawa, J. Phys. Chem. B. 107 (2003) 597-606.

[17] C.R. Zhang, Z.J. Liu, Y.H. Chen, H.S. Chen, Y.Z. Wu, L.H. Yuan, J. Mol. Struct. 899 (2009) 86-93.